ENCIT 2018

ABCM Associação Brasileira de Engenharia e Ciências Mecânicas

17th Brazilian Congress of Thermal Sciences and Engineering
November 25th-28th, 2018, Águas de Lindóia, SP, Brazil

# ENCIT-2018-0500
# DIRECT NUMERICAL SIMULATION OF VACILLATION IN CENTRIFUGAL CONVECTION

**Diogo B. Pitz**
**Olaf Marxen**
**John Chew**
Thermo-fluid Systems University Technology Centre
Mechanical Engineering Sciences
University of Surrey
Guildford, United Kingdom
d.bertapitz@surrey.ac.uk

***Abstract.*** *In rotating systems characterised by a constant angular velocity, i.e. without differential rotation, buoyancy effects occur if a temperature gradient is imposed. In particular, if the centrifugal acceleration induced by rotation is large enough, buoyancy effects in the radial direction compete with those induced by gravity, and in many cases the centrifugal force alone dominates the buoyant flow dynamics. In this study flow in a rotating, differentially heated cylindrical annulus is studied by means of direct numerical simulation (DNS), where the temperature at the outer cylinder is higher than that at the inner cylinder, and the flow is induced by buoyancy effects arising from the centrifugal force. This configuration is relevant in industrial applications, such as compressor cavities of turbomachinery internal air systems, and also in flows of geophysical interest. From previous work it is known that convection first starts in the form of nearly-circular counter-rotating rolls which span the entire axial length of the cavity, and also that at low Rayleigh numbers Ra the flow is dominated by a single azimuthal mode, whereas at high Ra broadband effects dominate. In this study the Rayleigh number is increased progressively and we investigate mode interactions that occur during the vacillation regime, which eventually lead the flow to a turbulent state.*

***Keywords:*** *centrifugal convection, rotating cavities, transition to turbulence, direct numerical simulation, high-order methods*

## 1. INTRODUCTION

In order to increase the efficiency of jet engines, it is desirable to operate at high compressor pressure ratios. A high pressure ratio implies that the air entering the engine core will reach a higher temperature at the compressor exit, therefore the possibility of a pressure ratio increase relies on the use of materials capable of tolerating high temperatures and on the use of efficient cooling systems. In modern jet engines an internal air system, also referred to as a secondary air system, is employed to cool certain engine components. An example of such a system for a compressor is shown schematically in Fig. 1(a). The air used in the internal air system is bled from the compressor and then used to cool the compressor disks. An accurate prediction of the disk temperatures is of great importance to control the thermal stresses. Additionally, the amount of thermal expansion of the disks controls the blade tip clearances, i.e., the distance between the tip of the compressor blades and the outer shroud (Owen and Long, 2015).

Since the air entering the inter-disk cavities is generally cooler than the outer part of the cavities, which is heated since the shroud is in contact with the air passing through the compressor blades, the flow is strongly affected by buoyancy effects. Such flows are inherently unsteady and therefore quite challenging to predict with the standard CFD tools used in the gas turbine industry. A complete description of the flow structure can only be obtained using unsteady CFD, and to date it is not clear whether meaningful results can be obtained with RANS-based turbulence models. For this reason, the use of high-fidelity simulations is crucial to improve the understanding of these flows.

To isolate the effect of centrifugal buoyancy on the flow inside the cavities shown in Fig. 1(a), it is useful to consider a simplified geometrical model consisting of a cylindrical annulus bounded by two parallel disks, as shown in Fig. 1(b), where the shroud (outer cylinder) is hotter than the shaft (inner cylinder). While this configuration neglects the effect of an axial throughflow that is encountered in modern jet engines, it contains the basic ingredients necessary to study the physics of buoyant flows in rotating cavities, namely rotation, which induces a centrifugal force directly radially outwards, and a radial temperature gradient. Additionally, it is worth noting that the cylindrical annulus is commonly used in numerical and experimental investigations of geophysical flows, such as convection in the core of planets and circulation of the

Earth's atmosphere (the interested reader may consult Read *et al.* (2014) and Früh (2014)). It should be noted that, in general, for these flows it is also necessary to consider the effect of axial gravity in the annulus, which gives rise to a baroclinic instability and thus different dynamics are encountered. However, the case of purely centrifugal convection can be seen as a limiting case of these configurations if the centrifugal acceleration exceeds that of gravity (see, e.g. Read *et al.* (2008)).

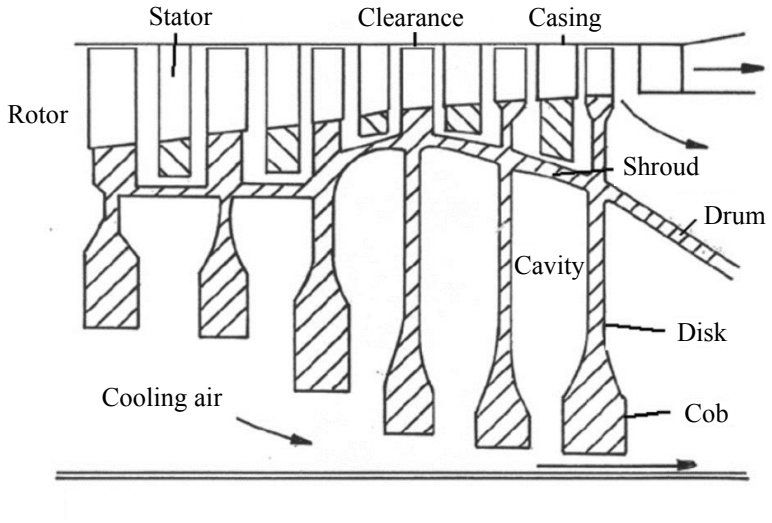


(a)

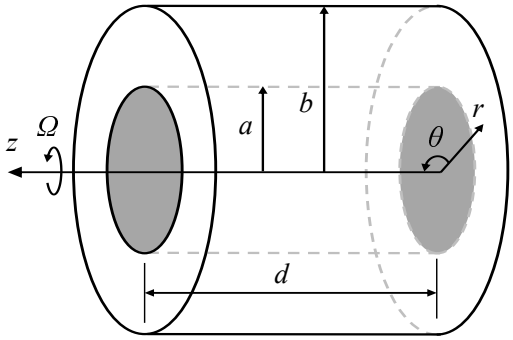


(b)

Figure 1: (a) Schematic representation of an internal air system. Figure from Owen and Long (2015). (b) Simplified geometry of a sealed rotating cavity.

At engine conditions, the centrifugal Rayleigh number inside compressor cavities is very high, such that the flow is chaotic. Still, studying the linear regime of convection and the stages of transition to turbulence is important to understand the basic instability mechanisms that govern the flow.

In our previous work (Pitz *et al.*, 2017) the onset of convection in a sealed rotating annulus was studied using linear stability analysis and direct numerical simulation (DNS). The analyses revealed that the convective state becomes unstable to nearly-circular pairs of convection cells, with alternating positive and negative temperature perturbations. Using DNS, it was observed that triadic interactions occur before energy saturation, and that these cause a change in the mode shapes associated with the azimuthal modes that participate in these interactions. At a relatively small Rayleigh number $Ra = 10^5$, the solution was dominated by a single azimuthal mode and its harmonics, which is characteristic of laminar flows. At $Ra = 10^8$, the flow was turbulent, as evidenced by the azimuthal energy spectrum, which revealed an energy distribution across multiple spatial scales.

Here, the study presented by Pitz *et al.* (2017) is extended to analyse intermediate transitions that occur between $Ra = 10^5$ and $Ra = 10^8$, and how these affect the flow structure and heat transfer. This is accomplished by performing several DNS for different values of the Rayleigh number and monitoring the flow variables at certain locations inside the cavity.

## 2. METHODOLOGY

Consider a sealed cylindrical annulus filled with air ($Pr = 0.7$), rotating at a uniform angular speed $\Omega$, with temperatures $T_a$ and $T_b$ at $r = a$ and $r = b$, respectively, such that $T_b > T_a$. A no-slip condition is applied on all surfaces, and the disks are adiabatic, i.e. $\partial_z T = 0$ for $z = 0$ and $z = d$. The effect of gravity is neglected, so that buoyancy is induced by the centrifugal force which arises due to the system rotation. The flow is governed by the Prandtl number $Pr$, the centrifugal Rayleigh number $Ra$, and the rotational Reynolds number $Re$, given by,

$$Pr = \frac{\nu}{\kappa}, \tag{1}$$

$$Ra = \frac{\Omega^2 r_m \alpha \Delta T (b-a)^3}{\nu\kappa}, \tag{2}$$

$$Re = \frac{\Omega r_m (b-a)}{\nu}, \tag{3}$$

where $\nu$ is the kinematic viscosity, $\kappa$ is the thermal diffusivity, $r_m = (b+a)/2$ is the mean radius, $\alpha$ is the thermal expansion coefficient, and $\Delta T = T_b - T_a$. In the analyses presented the Prandtl number is constant, $Pr = 0.7$, and $\alpha\Delta T = 0.1$, so that the Rayleigh and Reynolds numbers change simultaneously when the angular velocity is varied. The radius ratio $\eta = a/b$ is fixed at $\eta = 0.52$.

### 2.1 Governing equations

The flow is governed by the Navier-Stokes equations written in incompressible form, therefore the Mach number is assumed to be small. Buoyancy effects are accounted for using the Boussinesq approximation, in which it is assumed that density variations are negligible, except if they are multiplying a term that generates buoyancy, and also that the density varies linearly with the temperature, $\rho(T) = \rho_0 \left[1 - \alpha(T - T_a)\right]$. A non-inertial reference frame rotating at angular speed $\Omega$ around the $z$ axis is considered, therefore the Coriolis and centrifugal forces enter the equations explicitly, and a variable density is considered on the centrifugal force only. Thus, the governing equations are,

$$\nabla \bullet \mathbf{u} = 0, \tag{4}$$

$$\frac{\partial \mathbf{u}}{\partial t} + \mathbf{u} \bullet \nabla \mathbf{u} = -\nabla p^* + \nu \nabla^2 \mathbf{u} - 2\boldsymbol{\Omega} \times \mathbf{u} + \alpha(T - T_a)\boldsymbol{\Omega} \times (\boldsymbol{\Omega} \times \mathbf{r}), \tag{5}$$

$$\frac{\partial T}{\partial t} + \mathbf{u} \bullet \nabla T = \alpha \nabla^2 T. \tag{6}$$

In the equations above, $\mathbf{u}$ denotes the velocity vector in a cylindrical coordinate system and $p^*$ is the reduced pressure, which comprises both the static pressure and the constant part of the centrifugal force. Note that, since the angular velocity has a single component (in the axial direction), the last term of Eq. 5 is non-zero in the radial direction only.

### 2.2 Numerical method

The system of equations (4) – (6) is solved using a spectral element–Fourier method, employing a modified version of the code *Semtex*, described by Blackburn and Sherwin (2004). Spectral element formulations are obtained by discretising the governing equations in integral form using a Galerkin formulation and employing high-order polynomial expansion bases within each element. Generally, the polynomial expansion basis corresponds to a Lagrange polynomial interpolated at a given set of nodes. In particular, the choice of Gauss-Lobatto-Legendre (GLL) nodes is attractive within the context of nodal spectral element formulations, since they are able to provide spectral convergence for smooth solutions, are efficient for Gaussian quadrature integration and can be calculated numerically using recursive formulas.

Spectral and high-order methods provide lower dispersion and diffusion errors than low-order methods, and provide better accuracy per degree of freedom, particularly for long time integration periods. These properties are favourable in the context of numerical simulation of turbulent flows, where good accuracy is desirable to resolve all the relevant scales, such that uncontrolled artificial dissipation induced by the grid and numerical scheme can significantly compromise the solution quality. For further details, the reader may consult Karniadakis and Sherwin (2013).

Since the geometry used in this study is homogeneous along the azimuthal direction, the domain is discretised using a Fourier series expansion along $\theta$, whereas the $r - z$ plane is discretised using two-dimensional spectral elements. A second-order, semi-implicit, stiffly stable scheme is used for time integration, where the viscous terms are discretised implicitly in time, whereas the convective term and the Coriolis and centrifugal terms are integrated explicitly.

## 3. RESULTS AND DISCUSSION

Figure 2 shows the value of the Nusselt number, $Nu$, which is the ratio of convective and conductive heat transfer, on the outer cylindrical surface, for different values of the Rayleigh number. Note that the filled circles correspond to average values, whereas the crosses indicate points of minimum and maximum values observed over time for each $Ra$. The results indicate that, at low $Ra$, $Nu$ is steady, at intermediate $Ra$ it is time-periodic, and at high values of $Ra$ it shows a chaotic behaviour. This is further illustrated in Fig. 3, which shows phase space plots of the Nusselt number for different $Ra$. For $Ra = 4 \times 10^4$, the curve converges to a point after a short transient, indicating that $Nu$ is steady. For $Ra = 7.25 \times 10^4$ the flow becomes periodic, and is thus represented by a closed curve in the phase space diagram. It is interesting to note, from Fig. 2, that the mean value of the Nusselt number decreases slightly as $Ra$ is increased when the flow becomes time-periodic. For $Ra = 1.8 \times 10^5$, Fig. 3(c) reveals that the flow is still time-periodic, however for $Ra = 1.9 \times 10^5$ periodicity is lost, and the evolution of $Nu$ over time suggests that the flow is in a modulated amplitude vacillation regime, where chaotic behaviour starts to emerge.

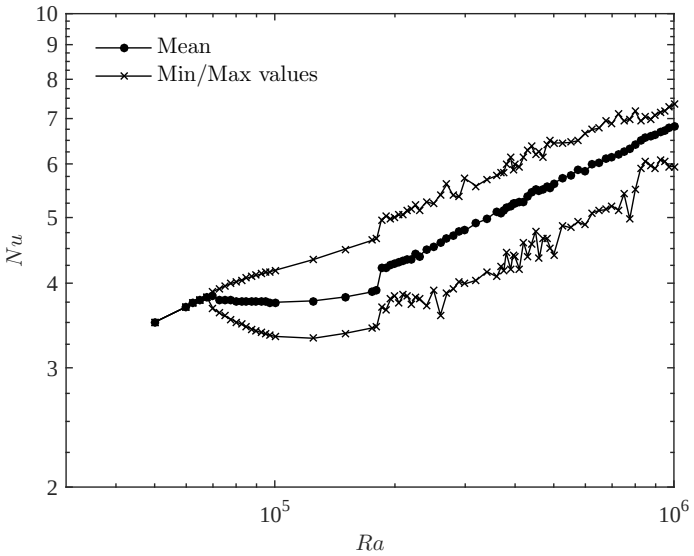


Figure 2: Nusselt number as a function of the Rayleigh number.

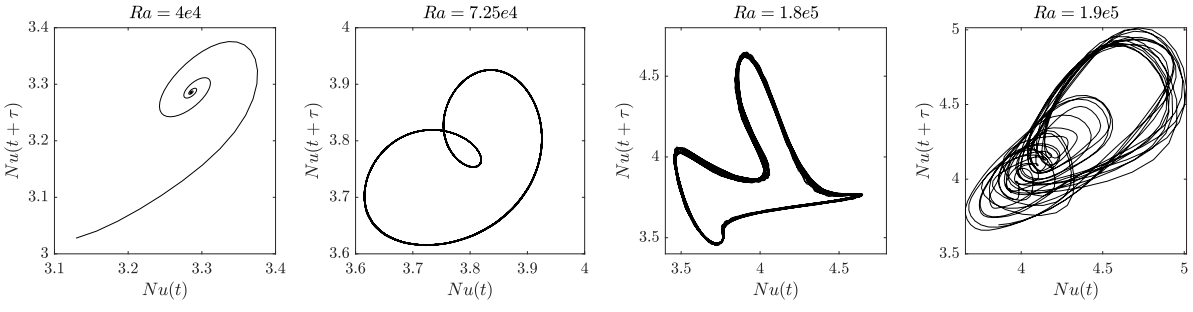


(a) (b) (c) (d)

Figure 3: Phase space diagrams of the Nusselt number at the outer cylindrical surface, for $Ra = 4 \times 10^4$, $Ra = 7.25 \times 10^4$, $Ra = 1.8 \times 10^5$ and $Ra = 1.9 \times 10^5$, respectively.

Note that in the transition from time-periodic to modulated amplitude vacillation behaviour, which occurs between $Ra = 1.8 \times 10^5$ and $Ra = 1.9 \times 10^5$, a step increase in the Nusselt number is observed, as shown in Fig. 2. This sudden increase is accompanied by a change in the flow structure, or more specifically, by a change in the dominant azimuthal wavenumber, which corresponds to the number of pairs of convection cells observed in the $r - \theta$ plane. This is illustrated in Fig. 4, which shows azimuthal energy spectra obtained for $Ra = 1.8 \times 10^5$ and $Ra = 1.9 \times 10^5$. Note that for $Ra = 1.8 \times 10^5$ the flow is dominated by $k_d = 6$, which is the wavenumber with highest energy at the start of the simulation, and its harmonics, while the energy of the remaining modes is essentially zero. When $Ra = 1.9 \times 10^5$, $k_d = 5$ dominates the spectrum, however the results also suggest that energy is transferred to sideband modes. As $Ra$ is further increased, the energy associated with these sideband modes increases substantially, such that broadband effects

eventually dominate the dynamics and the flow becomes chaotic, or turbulent. For $Ra$ up to $\approx 8 \times 10^5$, $k_d = 5$ is still the dominant mode, but above this value the flow transitions to $k_d = 4$, and a slight increase in $Nu$ is observed, cf. Fig. 2.

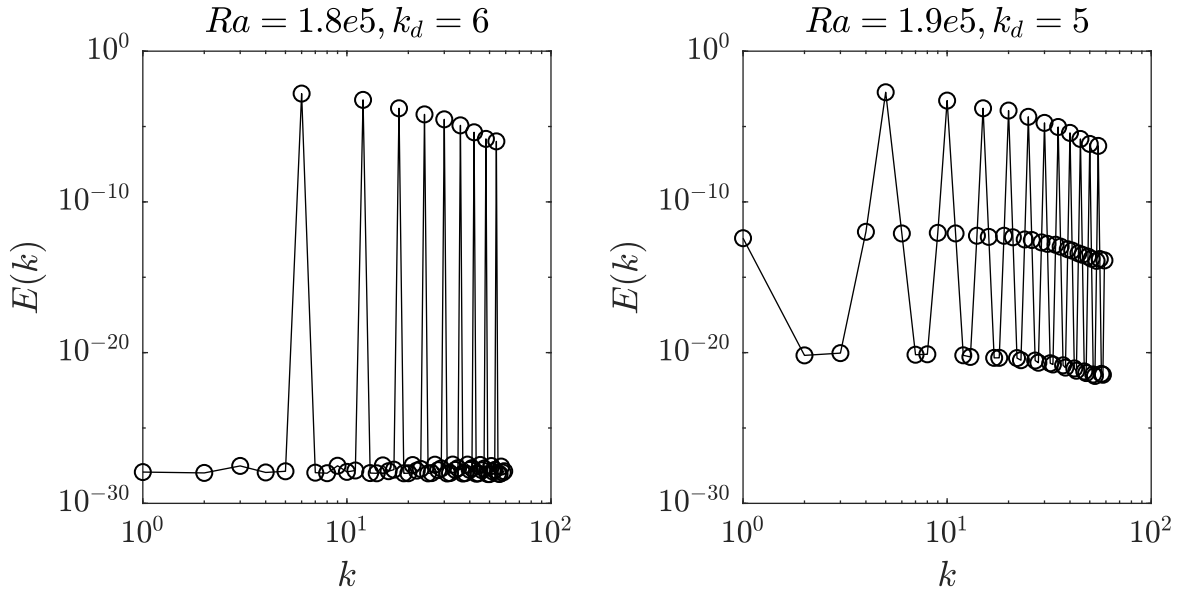


(a) (b)

Figure 4: Azimuthal energy spectra for $Ra = 1.8 \times 10^5$ and $Ra = 1.9 \times 10^5$.

## 4. CONCLUSIONS

In this paper the transition between different flow states in a differentially heated rotating annulus was investigated using direct numerical simulation, through a gradual increase of the centrifugal Rayleigh number. It was shown that at a certain value of the Rayleigh number a step increase in the Nusselt number occurs, which is accompanied by a change in the dominant azimuthal wavenumber from $k_d = 6$ to $k_d = 5$. In our previous study (Pitz *et al.*, 2017) a linear stability analysis revealed that the conductive base state loses stability to pairs of counter-rotating convection cells with azimuthal wavenumber $k_d = 5$, thus it is interesting to observe a change to this same wavenumber in the non-linear regime. For $Ra > 8 \times 10^5$, a transition to $k_d = 4$ occurred and persisted up to $Ra = 10^8$. In our previous study solutions with $k_d = 5$ at $Ra = 10^8$ were observed, however in that case a direct path from the conductive state was used, whereas in the present study $Ra$ was increased in a gradual fashion. This indicates that $k_d$ depends on the flow history, and that solutions with different $k_d$ may coexist, but it is important to note that $Nu$ is not affected by $k_d$ at such high values of $Ra$. The fact that $Nu$ increases during the wavenumber transitions, especially at low $Ra$, suggests that the flow organises itself so as to maximise the heat transfer from/to the cylindrical walls.

## 5. ACKNOWLEDGEMENTS

D. B. Pitz acknowledges the financial support provided by the CAPES foundation, grant no. 13.507/13-3.

## 6. REFERENCES

Blackburn, H.M. and Sherwin, S., 2004. "Formulation of a Galerkin spectral element–Fourier method for three-dimensional incompressible flows in cylindrical geometries". *Journal of Computational Physics*, Vol. 197, No. 2, pp. 759–778.

Früh, W.G., 2014. "Amplitude vacillation in baroclinic flows". In T. von Larcher and P.D. Williams, eds., *Modeling Atmospheric and Oceanic Flows: Insights from Laboratory Experiments and Numerical Simulations*, John Wiley & Sons.

Karniadakis, G. and Sherwin, S., 2013. *Spectral/hp element methods for computational fluid dynamics*. Oxford University Press.

Owen, J.M. and Long, C.A., 2015. "Review of buoyancy-induced flow in rotating cavities". *Journal of Turbomachinery*, Vol. 137, No. 11, p. 111001.

Pitz, D.B., Marxen, O. and Chew, J.W., 2017. "Onset of convection induced by centrifugal buoyancy in a rotating cavity". *Journal of Fluid Mechanics*, Vol. 826, pp. 484–502.

Read, P.L., Maubert, P., Randriamampianina, A. and Früh, W.G., 2008. "Direct numerical simulation of transitions towards structural vacillation in an air-filled, rotating, baroclinic annulus". *Physics of Fluids (1994-present)*, Vol. 20, No. 4, p. 044107.

Read, P.L., Pérez, E.P., Moroz, I.M. and Young, R.M., 2014. "General circulation of planetary atmospheres: Insights from rotating annulus and related experiments". In T. von Larcher and P.D. Williams, eds., *Modeling Atmospheric and Oceanic Flows: Insights from Laboratory Experiments and Numerical Simulations*, John Wiley & Sons.

## 7. RESPONSIBILITY NOTICE

The authors are the only responsible for the printed material included in this paper.